Fiber-Based Composite Meshes with Controlled Mechanical and Wetting Properties for Water Harvesting

Joanna Knapczyk-Korczak[1], Daniel P. Ura[1], Marcin Gajek[2], Mateusz M. Marzec[3], Katarzyna Berent[3], Andrzej Bernasik[3,4], John P. Chiverton[5], Urszula Stachewicz[1]*

[1]Faculty of Metals Engineering and Industrial Computer Science, International Centre of Electron Microscopy for Materials Science, AGH University of Science and Technology, Poland
[2]Faculty of Materials Science and Ceramics, AGH University of Science and Technology, Poland
[3]Academic Centre for Materials and Nanotechnology, AGH University of Science and Technology, Poland
[4]Faculty of Physics and Applied Computer Science, AGH University of Science and Technology, Poland
[5]School of Energy and Electronic Engineering, University of Portsmouth, Portsmouth, United Kingdom

*Corresponding author: Urszula Stachewicz

E-mail: ustachew@agh.edu.pl; Tel.: +48 12 617 52 30

Keywords: electrospinning, fiber, composite, hydrophobic, hydrophilic, wetting, roughness, mechanical properties, fog collectors, water, PA6, PS

Abstract:

Water is the basis of life in the world. Unfortunately, resources are shrinking at an alarming rate. The lack of access to water is still the biggest problem in the modern world. The key to solving it is to find new unconventional ways to obtain water from alternative sources. Fog collectors are becoming an increasingly important way of water harvesting as there are places in the world where fog is the only source of water. Our aim is to apply electrospun fiber technology, due to its high surface area, to increase fog collection efficiency. Therefore, composites consisting of hydrophobic and hydrophilic fibers were successfully fabricated using a two-nozzle electrospinning set up. This design enables the realization of optimal meshes for harvesting water from fog. In our studies we focused on combining hydrophobic, polystyrene (PS) and hydrophilic, polyamide 6 (PA6) surface properties in the produced meshes, without any chemical modifications, based on new hierarchical composites for collecting water. This combination of hydrophobic and hydrophilic material cause water to condense on the hydrophobic microfibers and to run down on the hydrophilic nanofibers. By adjusting the fraction of PA6 nanofibers we were able to tune the mechanical properties of PS meshes and importantly increase the efficiency in collecting water. We combined a few characterization methods together with novel image processing protocols for the analysis of fiber fractions in the constructed meshes. The obtained results show a new single-step method to produce meshes with enhanced mechanical properties and water collecting abilities that can be applied in existing Fog Water Collectors. This is a new promising design for fog collectors with nano- and macro- fibers which are able to efficiently harvest water, showing a great application in comparison to commercially available standard meshes.

1. INTRODUCTION

There are places in the world where fog is the only source of water and collecting it gives many species, that includes humans, a higher chance of survival[1,2]. Fog is also used for the extensive studies of pollution especially in many regions in Asia[3]. In terms of catching fog water many studies have tried to biomimic various solutions that we can observe in nature, in relation to surface properties and topography[4,5]. Typical fog collectors are spider webs from silk fibers decorated with spindle-knots. These have hydrophilic properties which are able to capture moisture from the air[6]. Similarly cactus (*Opuntia microdasys*) and Namib Desert beetles (*Stenocara gracilipes* and *Onymacris unguicularis*) are able to collect water from air using the surface of their body[7]. People observed this to create biologically inspired fog collectors to catch water from humid air[8]. Fog Water Collectors (FWC)s are nets built from fibers of a specially designed mesh[9]. This is a source of potentially clean water in parts of the world where conventional sources are unavailable or in short supply. The requirements of the environment, where FWCs can be built are relatively low. FWCs also need light winds to collect water in an effective way. They are designed to catch the tiny droplets of water liquid present in fog[10]. To improve efficiency of existing construction designs are applying a combination of hydrophilic and hydrophobic polymer fibers. The hydrophilic part of a FWC catches the water and the hydrophobic part drains it to the special reservoir, even when there are limited wind conditions[7].

There has been increasing interest in nanofibers across many domains of applied materials[11] including water harvesting applications as they increase the effective area of water collection[12]. To collect water, a fiber mesh is most often utilized due to its larger surface area and the possibility to a create hierarchical structure[13]. However, this is only one possibility. There are research studies in which different types of strips[14], wires[15], harps[16] or mechanisms to mimic nature have been applied[17,18]. Additionally the microstructure effect on the

coalescence of water droplets responsible for improving water harvesting from polydimethylsiloxane (PDMS) films have also been investigated[19]. Water condensation performance according to the hierarchical roughness on metallic coatings was also analyzed in terms of water drops adhesion and nonwetting effects[20]. To direct droplets to a FWC electric fields can be used if the natural movement of air is insufficient[21]. The standard FWCs are usually made of polymers such as polypropylene (PP)[8]. This gives a lot of flexibility when relying on the natural wind force to enhance droplet deposition from fog[22,23]. The efficiency of collecting water structures based on nanofibers can be increased by modifying them or by creating composites combining fibers with different properties[24,25]. Electrospinning is a versatile method allowing us to use a multi nozzle set-up[26]. Another option is to use two unconnected nozzles[27] and electrospinning two different polymers at the same time or one by one to produce a layered structure.

In our research studies we focus on using electrospun fibers, in terms of combining hydrophobic and hydrophilic surface properties without any chemical modifications. This way we want to follow the principle designs observed in nature for water harvesting purposes. We have successfully produced various nanofiber meshes from hydrophobic polystyrene (PS) and hydrophilic polyamide 6 (PA6). Combining these two polymers, we have managed to produce new hierarchical composites for collecting water. The various designs with the controlled hydrophilic fraction were investigated in terms of their wetting and mechanical properties. These are crucial to construct effective fog collectors. By adjusting the fraction of PA6 nanofibers we are able to tune the mechanical properties of PS meshes and increase water collection efficiency. We combine a number of characterization methods together with novel image processing protocols for the analysis of fiber fractional contributions in the constructed meshes. The obtained results show a new single-step method to produce meshes with the enhanced water collecting abilities. This is a very promising pathway to design fog collectors with nano- and macro- fibers without any chemical modification of mesh surfaces. Finally, we compare the efficiency in collecting water using various designs of electrospun composite

meshes at the laboratory scale experiments with the commercially available Raschel meshes. Our electrospun fiber composites in combination with the Raschel meshes show a great potential application in FWCs to enhance water collection efficiency in various methodological conditions even including low wind speed.

2. EXPERIMENTAL METHODS

2.1 Materials

The polymer solutions were prepared at an ambient temperature (20^{o}C) on a magnetic stirrer plate for 4 h at 500 rpm (IKA RCT basic, Germany). Prior to the solution preparation the two polymers: polystyrene (PS, Sigma Aldrich, UK, M_w = 350000 g·mol^{-1}) and polyamide 6 (PA6, BASF, Germany, M_w = 24 000 g·mol^{-1}), were dried at a temperature of 30 ºC for 3 h to constant weight. Next, the PS was dissolved in dimethylformamide (DMF, 99.8%, POCH, Poland) at 25%$_{wt.}$ and PA6 was dissolved in a mixture of acids: formic acid (85%) and acetic acids (99.5%) with volume ratio 1:1 (POCH, Poland) at 12%$_{wt.}$

2.2 Electrospinning

PS and PA6 fibers were produced via electrospinning in the configuration listed in Table 1 (Apparatus EC-DIG with Climate-control – IME Technologies, the Netherlands) at T=25^{o}C and H=40% with other parameters listed in Table 2. The schematic of the electrospinning set-up with two nozzles is shown in Figure 1. The composites of PS and PA6 were randomly deposited on the slowly rotating drum at 10 rpm. Composites were electrospun from two nozzles simultaneously (at the same time) and with the layer by layer method. The thicknesses of the fiber layers were controlled with the electrospinning depositing time.

Table 1. The list of the composite designs with electrospun fibers from PS and PA6, including the production details and abbreviations.

No	Electrospinning method	Electrospinning time of PS [min]	Electrospinning time of PA6 [min]	Abbreviations of the composite type
1.	Simultaneous electrospinning from two nozzles	-	-	**PS-PA6**
2.	Simultaneous electrospinning from two nozzles + extra layer of PA6 on the top	-	+ 15 min extra on the top of the composite mesh	**PS-PA6+15**
3.	Electrospinning layer by layer	1	1	**PS(1)-PA6(1)**
4.	Electrospinning layer by layer	1	2	**PS(1)-PA6(2)**
5.	Electrospinning layer by layer	1	4	**PS(1)-PA6(4)**

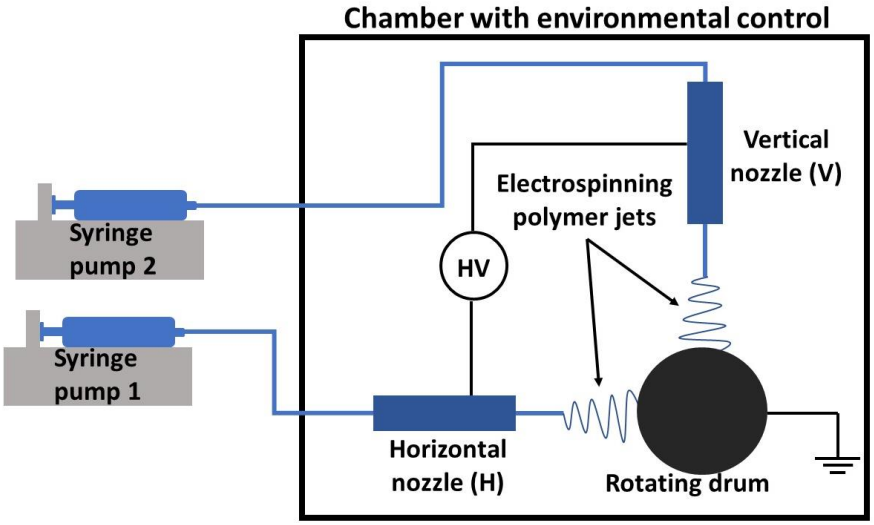

Figure 1. The scheme of electrospinning set-up with the environmental controlled chamber and two nozzles set horizontally (H) and vertically (V) to produce composite meshes from two different polymer fibers.

Table 2. Electrospinning parameters for PA6 and PS and PA6-PS composites, with 2 nozzles set-up, nozzle position H – horizontal, V – vertical.

Samples		Flow rate [ml·h^{-1}]	Distance [cm]	Voltage [kV]	Needle speed [mm·s^{-1}]	Nozzle position
PS fibers		1.5	15	12	20	H
PA6 fibers		0.2	15	16	20	H
Composite: 1. PS-PA6 2. PS-PA6+15	**PS**	1.5	15	12	20	H
	PA6	0.1	17		20	V
Composite: 3.PS(1)-PA6(1) 4.PS(1)-PA6(2) 5.PS(1)-PA6(4)	**PS**	5	17	13	15	V
	PA6	0.3	15	16	20	H

2.3 Microscopy and fiber fraction analysis

Fibers' morphology and diameters were analyzed by scanning electron microscope (SEM, Merlin Gemini II – ZEISS, Germany). Prior SEM imaging samples were coated with 5 nm of gold by rotary – pump sputter coater (Q150RS – Quorum Technologies, Laughton, UK). The average fiber diameters were measured on 100 fibers using Image J software (v.1.50i, National Institutes of Health, USA). The cross-sections of the composite samples were freeze fractured prior to imaging.

A different process was followed to estimate the volume fractions of the two fiber types. For the volume fractions, the fibers are detected here in a number of 2D SEM images using a scale dependent technique based on the Hessian matrix. The Hessian is calculated at every pixel for each SEM image. A Hessian matrix consists of second order derivatives of the image data that are calculated across all pixel locations. To help identify structures at different scales, scale dependent image smoothing is used prior to calculation of the second order derivatives. The eigenvalues of each of the Hessian matrices are then calculated and used to detect regions of an image with tubular structures. This approach has previously been used, in 3D, to detect electrospun fibers in X-ray CT images by *Chiverton et al.*[28]. It was originally

developed by *Frangi et al.*[29] to detect blood vessels and implemented in the Insight Toolkit (ITK) by *Antiga*[30]. However, the work here differs because it consists of two sets of fibers with different diameters. The detection process has therefore been adapted and involves detecting the relatively wider PS fibers at a greater scale. These larger fibers are more easily detected. However, the PA6 fibers are much thinner which can make fiber detection, at the same scale and resolution somewhat more challenging. Nevertheless, it was found that the thinner PA6 fibers could be isolated by, first detecting the fibers at a smaller scale using the Hessian fiber detection process with little to no image smoothing. Then masking out the regions of the image that correspond to the thicker fibers. The fiber detection processes, for the PS and PA6 fibers, result a set of two images. These images are then thresholded to produce a set of pixels that are used to estimate the volume presence of the two materials in the SEM image. This process was repeated across a range of different scales and different threshold levels using random sampling with a sample size of 200. Means and standard deviations estimates of the proportions of the two materials for each SEM image could then be produced

Additionally, the wetting observations of electrospun fibers were carried out using environmental SEM (ESEM) (FEI, Versa 3D, USA) including the Peltier stage set to -20°C – R.T. To carry out the measurement special frames were prepared with dimensions 10×10 mm with PS and PA6 fibers where we deposit very small droplets using spray brush (Aero-pro 30A, Harder & Steenbeck GmbH & Co.KG, Germany) and automatic pipette (Optipette 0.5-10 µL). Pressure in the chamber for PS and PA6 was respectively 113 and 134 Pa. The initial temperature was -17ºC to counteract the evaporation of water during waiting for the vacuum. The humidity in the chamber was 70% for PS and 83% for PA6 and the SEM microphotographs were obtained at 20 and 10 kV, respectively.

2.4 Surface chemistry and profilometry

The surface chemistry of electrospun polymer fibers was analyzed by the X-ray Photoelectron Spectroscopy (XPS, PHI VersaProbe II Scanning system) with monochromatic Al Kα (1486.6 eV) X-ray. The pass energy was set to 23.50 eV in the analyzer and the pressure in the chamber during analyzes was 4×10^{-9} mbar. The XPS method was used to investigate the fraction of PS and PA6 fibers in composites. The scan sample area was 400×400 μm and the photoelectron take – off angle was 90°.

For the profilometry study and roughness R_a measurements we used a laser microscope (Olympus OLS4000, Japan). Prior to the measurements, the electrospun fibers were deposited on a glass surface and covered with the 5 nm gold layer because the polymers can be transparent to light. The measured area for PS was 646×646 μm and for PA6 was 130×130 μm. We performed 10 measurements per sample enabling estimates of the means and standard deviations[31].

2.5 Mechanical testing

The mechanical properties were measured using a Tensile Module with 1 N Load Cell (Kammrath Weiss GmbH, Germany). The fiber mats placed in the frames 8×20 mm with cut sides. Then prior tensile testing, performed uniaxially was undertaken with a speed of 25 $\mu m \cdot s^{-1}$ (Figure S1 in the Supporting Information). We performed 5 tests per sample type. The thicknesses of all samples were measured using Image J software (version 1.50i, National Institutes of Health, USA) from the images taken with digital microscope Dino-Lite Digital Microscope (Dino-Lite Europe/IDCP B.V., The Netherlands). From the stress-strain curves, maximum stress and strain were calculated, together with toughness using Origin Integrate Function (OriginPro 2018b, version: b9.5.5.409, USA). The results are summarized in Table 3 and Figure 6.

2.6 Advancing and dynamic wetting contact angle

The advancing contact angle on the horizontally placed mats was measured (θ_s). This was used to determine the wetting properties of the electrospun fibers using deionized water (DI, Spring 5UV purification system – Hydrolab, Poland), glycerol (Anhydrous Pure, POCH, Poland) and formamide (ACS, Pure P.A, POCH, Poland). Droplets of 3µL volume were placed on the fibers using an automatic pipette (Optipette 0.5-10 µL) at laboratory conditions T=23°C and H=40%. The image of water droplets was taken 3 s after the deposition using a Canon EOS 700D camera with EF-S 60 mm f/2.8 Macro USM zoom lens. The contact angle was measured using Image J software (version 1.50i, National Institutes of Health, USA).

The dynamic water contact angle and hysteresis were measured from the droplets obtained on the meshes. This was done by positioning it vertically from the water vapor condensation. The images of water droplets were taken using the same camera set-up and the contact angle was measured using the same software as used for advancing contact angle measurements. The hysteresis was calculated as a difference between down and top contact angles. The effectiveness of the meshes in collecting water from humid air was verified with specially designed set-up showed in Figure 2. The humidity was controlled by conventional humidifier (Beurer GmbH, Germany) with flow efficiency 400 $ml \cdot h^{-1}$ and fog flow velocity of 19 $cm \cdot s^{-1}$. The polymer fiber meshes were placed on the special stand, covering the area of 100 cm^2 (10×10 cm) for all the samples. Water from the meshes was collected in the glass container placed underneath the frame. The mass of the collected water was checked every 30 min over a 3 h experiment at T=30ºC and H≈95%. The distance between the mesh and the orifice from the humidifier was set to 15 cm steaming the water vapor to the samples at the angle of 30º (Figure 2a). The efficiency of electrospun samples as a fog collector were calculated as the mass of water collected per unit area of the mesh. To check the influence of the distance and the angle of fog flow to efficiency of collecting water we repeated the experiment for the composite with the highest mechanical properties. The distance has been lowered to 6 cm[32] and the fog flow

was directed perpendicular to the mesh[14] (Figure 2b). Using the same parameters we checked the efficiency of collecting water for a commercial Raschel mesh which is often used in FWC constructions[33,34], see Figure S8 in the Supporting Information. The experiments were repeated a few times over various time frames with error based at 6% in water collection efficiency.

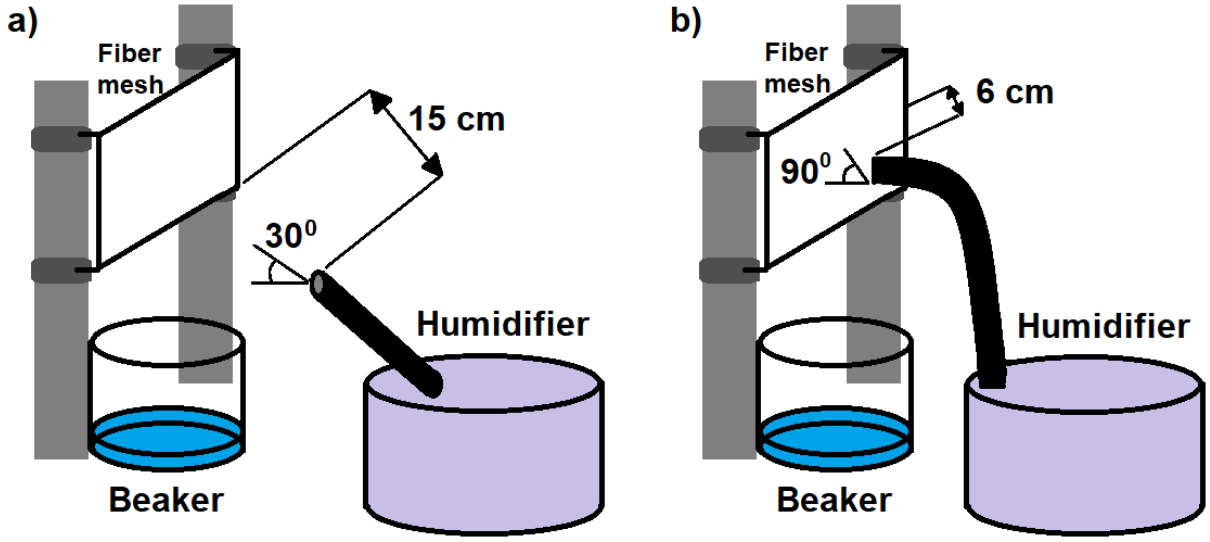

Figure 2. Schematics of the set-ups to collect water droplets from humid air on the electrospun meshes: a) distance of 15 cm and fog flow angle of 30º, b) distance of 6 cm and fog flow angle of 90º.

3. RESULTS AND DISCUSSION

3.1 Fibers morphology

The SEM images of PS and PA6 fibers showing their morphologies are included in Figure 3, together with histograms indicating fiber size distribution. The average fiber diameter of the PS fibers was 4.80 ± 0.22 µm and PA6 fibers was 0.11 ± 0.03 µm, similar to the previous study[31]. Both polymers were used to produce composites by electrospinning at the same time from two nozzles or layer by layer. Figure 4 includes SEM micrographs of each of the five types of the composite investigated. Observing across all the SEM images, it is clear the principal difference is in the fiber diameter creating hierarchical structure. The top view SEM images of PS-PA6 composites were also used for image processing including proportion of the PA6 fraction, what corresponds to the hydrophilic fraction in the composite meshes. The image processing results were further confirmed with XPS and roughness analysis of all the samples, see Figure 5. The hydrophilic part in the composite meshes, given by the PA6 nanofibers fraction, is responsible for wetting and mechanical properties. This is crucial for the fabrication of a reliable fog collector[10]. The static water contact angle on PS fibers meshes was 142.08 ± 1.71º and on PA6 was 44.60 ± 2.45º. In the case of the composites, the water contact angle is reduced with the increased fraction of PA6 to 122.93 ± 2.44º for the composite PS-PA6+15. Similarly, for the PS(1)-PA6(4), to 123.26 ± 1.82º. See Figure 5 and Tables S1 and S2 in the Supporting Information. The test with the deionized water were compared with the collected water from the rain. These showed comparable results, as can be seen in Figure S3 and Table S3 in the Supporting Information. Additionally, the wetting of PS and PA6 mats were verified using ESEM, as shown in Figure S4 in the Supporting Information. We were able to identify individual droplets on PS fibers and also the wetted regions between fibers. For the case of the PA6 nanofibers, only the wetted regions on the mats were visible. After wetting, the fiber morphology stayed unchanged, as the ESEM images show in Figure S5.

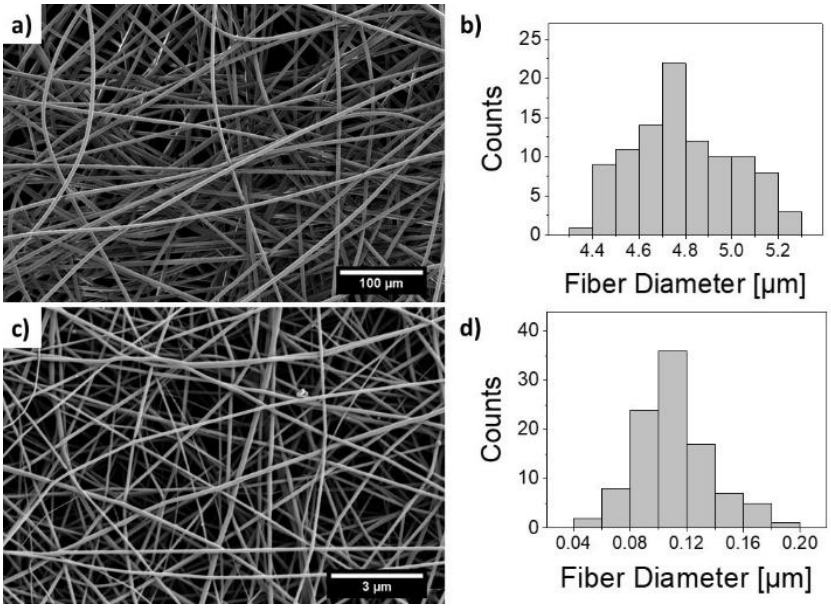

Figure 3. SEM micrographs of electrospun fibers and their fiber diameter histograms for a), b) PS and c), d PA6, respectively.

The fibrous composite samples were produced in two ways, electrospinning PS and PA6 at the same time and layer by layer, as indicated in Table 1. In Figure 4 the cross-sectional SEM images indicate the differences in the structure of the composite in relation also to the electrospinning time of PA6. Increased PA6 fractions reduces the electrostatic interaction between the PS fibers, resulting in more compact structures of the composites. The cross section of PS fibers reveals the internal porosity, as shown previously[35].

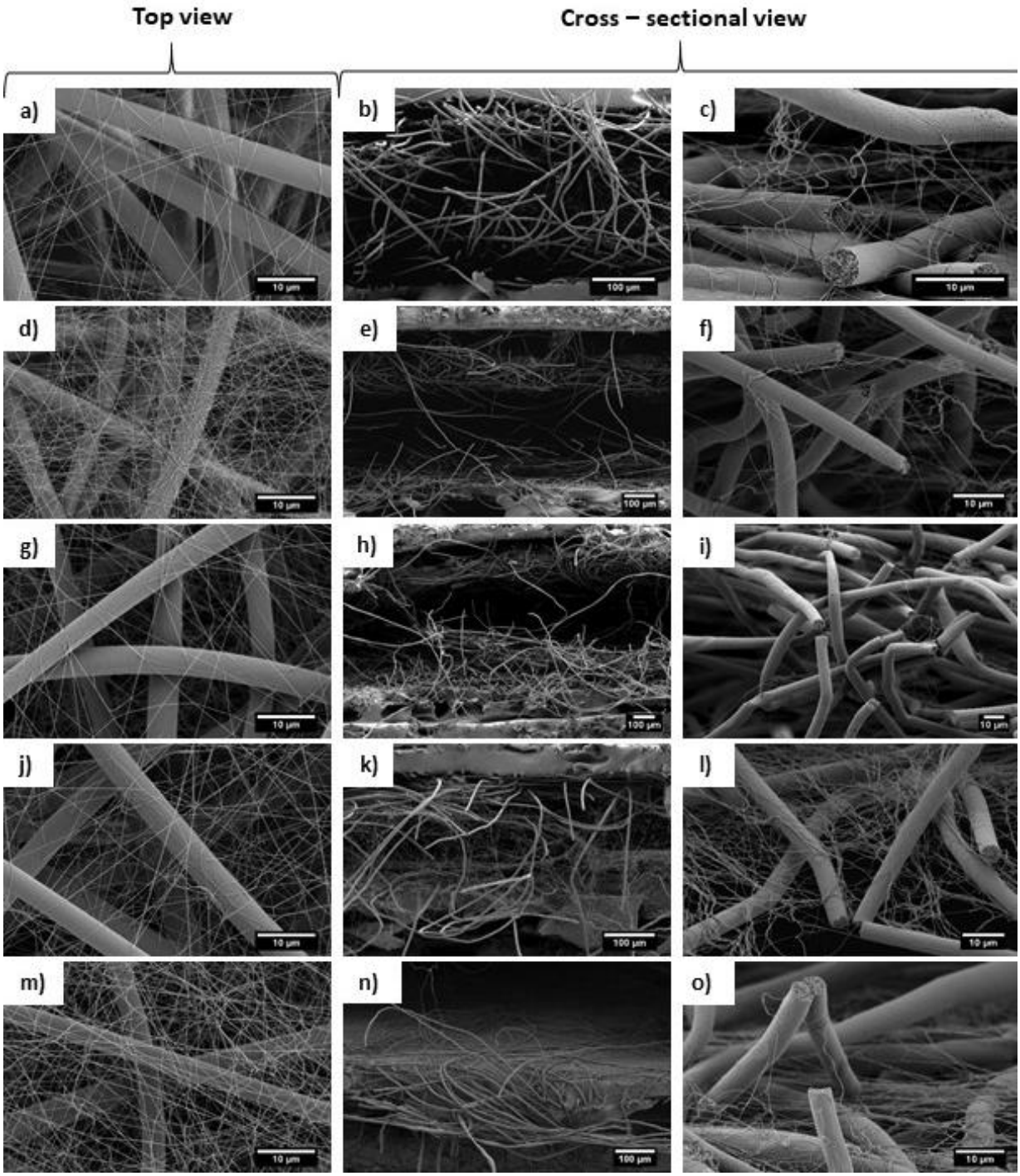

Figure 4. SEM micrographs of top and cross sectional view for the following sample of composite fibers: a, b, c) PS-PA6, d, e, f) PS-PA6+15, g, h, i) PS(1)-PA6(1), j, k, l) PS(1)-PA6(2), m, n, o) PS(1)-PA6(4).

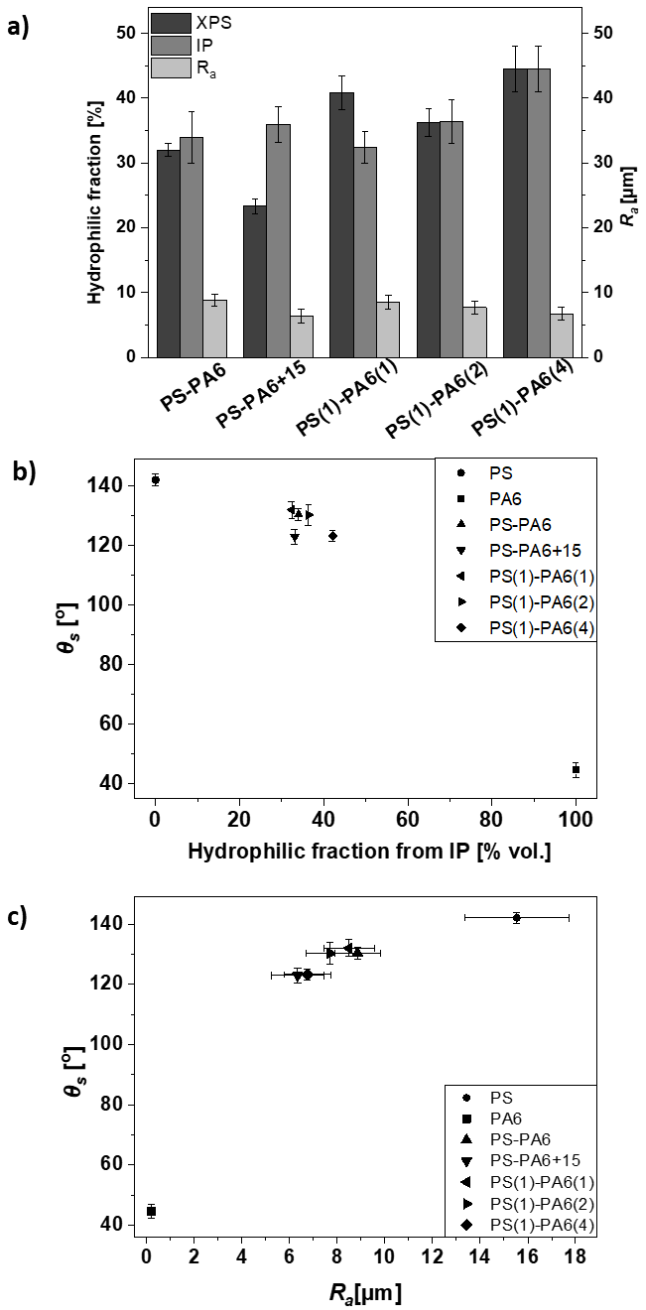

Figure 5. a) Calculated hydrophilic fraction in composites based on Image Processing Analyzed (IP), XPS results and roughness, R_a, for all electrospun samples, b) relation of static contact angle θ_s to hydrophilic fraction from IP analyze, c) dependence of θ_s to surface roughness.

Surface roughness was analyzed by a profilometry study. The images from the laser microscope show significant differences in surface roughness, R_a, of electrospun polymer fibers meshes, where the PS fibers resulted in greater roughness (R_a = 15.535 ± 2.197 µm) in comparison to the PA6 fibers (R_a = 0.205 ± 0.022 µm). See Figure S2 in the Supporting

Information and in Figure 5. The meshes from the PS fibers were very fluffy, like cotton wool, which was related to the repulsion between the PS fibers due to accumulated charge residues during electrospinning[36]. The PA6 fiber composites formed compact meshes with lower roughness than for the PS meshes. Similarly, for the composites containing a large fraction of PS fibers. Moreover, the longer time of electrospinning of the PA6 fibers, increased the hydrophilic fraction of the PA6 fibers and decreased the R_a in the composites, as shown in Figure 5a. The surface chemistry analysis via XPS confirms the majority of the image processing analysis, which are more accurate. This can be further extrapolated in terms of verification of PA6 nanofibers being responsible for the reduction of static contact angle[31,37,38], as shown in Figure 5. However, the increased fraction of PA6 in composites causes only a slightly lower water contact angle as the roughness also plays an important a role in the wetting[37,38].

3.2 Mechanical testing

The result from the mechanical tests are shown in Figure 6, indicating higher tensile stress values for PA6 nanofibers in comparison to PS microfibers, from 1.24 to 0.3 MPa for randomly oriented fibers. Therefore, the increased fraction of PA6, especially for the composites PS(1)-PA6(4) result in higher mechanical properties like toughness, maximum stress and strain at maximum stress, as showed in Table 3. PS fibers show very brittle behavior[39], however when the PA6 nanofibers were incorporated into the meshes, the maximum stress increased even more than 3.5 times. Only for the PS-PA6 composites, electrospun at the same time, the higher values were reported previously by *Li et al.*[40] and by *Yoon et al.*[26]. Generally, the greater the fraction of PA6 nanofibers, the greater the enhancement of the mechanical properties of the composite meshes. This is confirmed by the higher maximum stress levels obtained during the tensile testing, see Figure 6. Raschel meshes commonly used in FWCs have higher tensile strength, but they show very high anisotropy of mechanical properties[9]. The mechanical strength of the mesh ranges from 1000 to 3500 $N \cdot m^{-1}$

depending on the stretching direction and the elongation is between 20% and 100%. These nets often have to withstand very strong winds because they are installed in the areas where wind can reach speeds of 70 $m \cdot s^{-1}$. The electrospun fibers can be incorporated into the mesh of existing FWC e.g. a Raschel mesh, which would help to reduce the anisotropy and even further increase their mechanical strength.

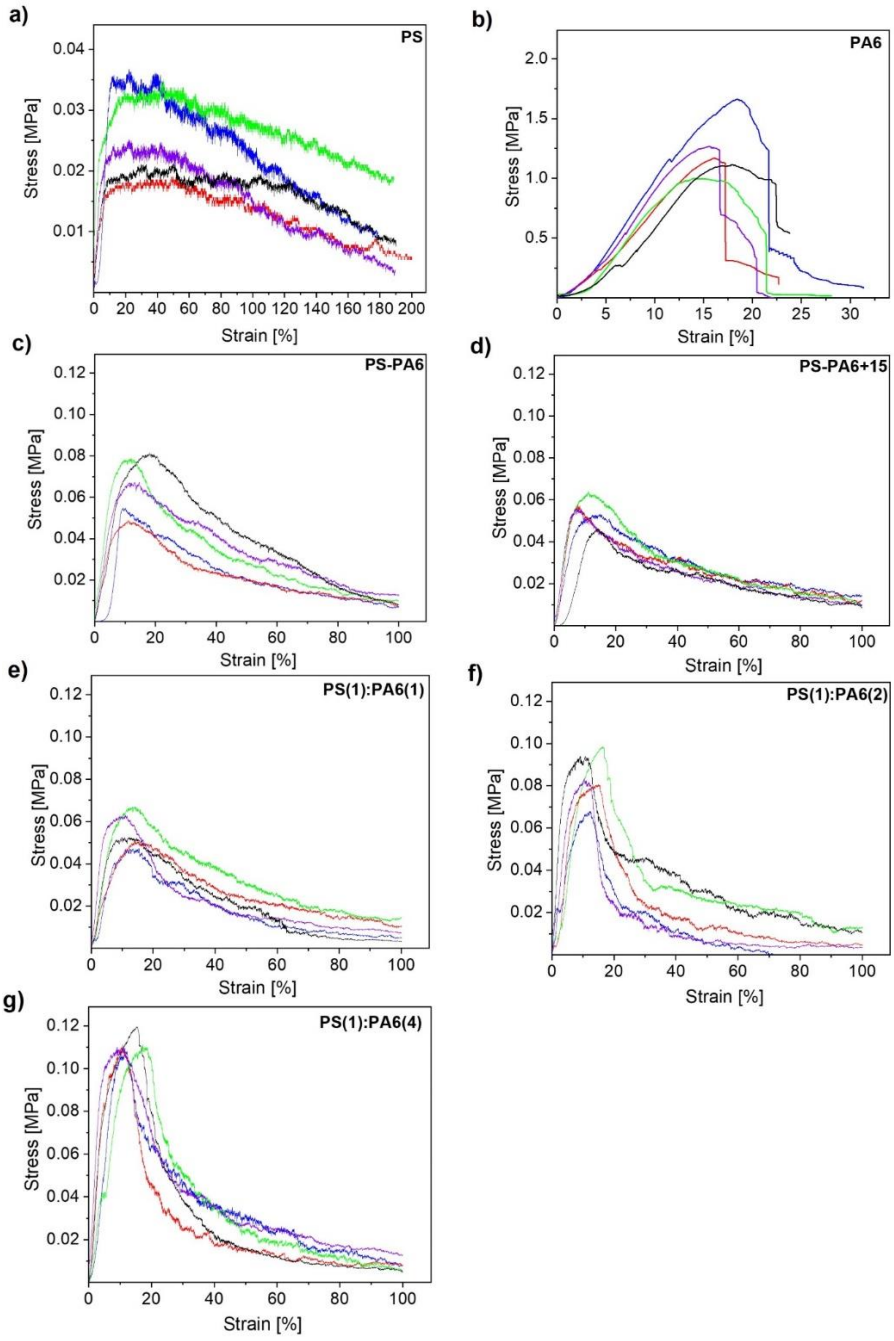

Figure 6. The stress-strain curves for randomly oriented fiber mats and composites from tensile test of a) PS, b) PA6, c) PS-PA6, d) PS-PA6+15, e) PS(1)-PA6(1), f) PS(1)-PA6(2), g) PS(1)-PA6(4) samples.

Table 3. Summary of all mechanical properties of electrospun fiber and composites meshes.

Samples	**Max. stress [MPa]**	**Strain at max. stress [%]**	**Toughness [MJ·m^{-3}]**
PS	0.03 ± 0.01	37.35 ± 12.54	3.51 ± 0.92
PA6	1.24 ± 0.23	16.46 ± 1.59	15.21 ± 3.76
PS-PA6	0.07 ± 0.01	12.97 ± 3.07	3.41 ± 0.71
PS-PA6+15	0.06 ± 0.01	11.11 ± 2.99	3.19 ± 0.38
PS(1)-PA6(1)	0.06 ± 0.01	12.97 ± 2.01	2.76 ± 0.64
PS(1)-PA6(2)	0.08 ± 0.01	13.02 ± 2.34	2.51 ± 1.01
PS(1)-PA6(4)	0.11 ± 0.01	13.14 ± 2.57	3.59 ± 0.44

3.3 Collecting water from the humid air

The water was collected in the controlled conditions over 3 h in the beaker placed under the tested samples mounted on the special stand, as shown in Figure 2 a). In the photographs in Figure 7 and Figure S6 in the Supporting Information the straight forward differences in shape and size of the droplets on all the different types of samples can be observed. During the water collecting experiment the fibers in meshes have not been damaged, Figure S7 in the Supporting Information. Clearly, the droplet shapes and wetting vary on the hydrophobic PS and hydrophilic PA6 meshes and the various fractions of hydrophilic fibers. The close-up pictures were used to calculate the contact angle hysteresis in collected water droplets on vertically placed meshes. The contact hysteresis was obtained for the composite meshes with the lower roughness, i.e. with higher amounts of hydrophilic PA6 nanofibers, and all the values are plotted in Figure 8a. According to previous studies, lower contact angle hysteresis improves the water collecting process, which was showed on PVDF-HFP nanomat impregnated with lubricants (Krytox-1506)[32]. However, the high contact angles which also represent low contact

angle hysteresis, have a tendency to stay on the meshes and block the flow of the humid air, showing lower efficiency in collecting water.

The contact angle hysteresis for our composite meshes was changing over the collection time. It decreased, particularly in contrast to PS meshes, as indicated in Figure 8a. Importantly, we observed also a lowering in contact angle hysteresis for composites meshes over the collecting time that was enhancing the water collecting efficiency. In case of the flattened droplet shapes for composites, Figure 7, we noticed much lower contact angle hysteresis. Moreover, the water was not penetrating the PS meshes as is the case for PA6 fibers, as was it was observed as a darker spot on ESEM images, see Figure S4 in the Supporting Information and Figure 7 b. For PA6 meshes we measured the contact angle hysteresis in the first 90 min over the total time of the experiment, as the water was soaking inside the mesh.

Importantly, including PA6 nanofibers we lowered the roughness of the meshes and the static contact angle, see Figure 2S and Table 1S in the Supporting Information. The increased roughness increased also the hydrophobicity of the meshes [37,41, 42,43].

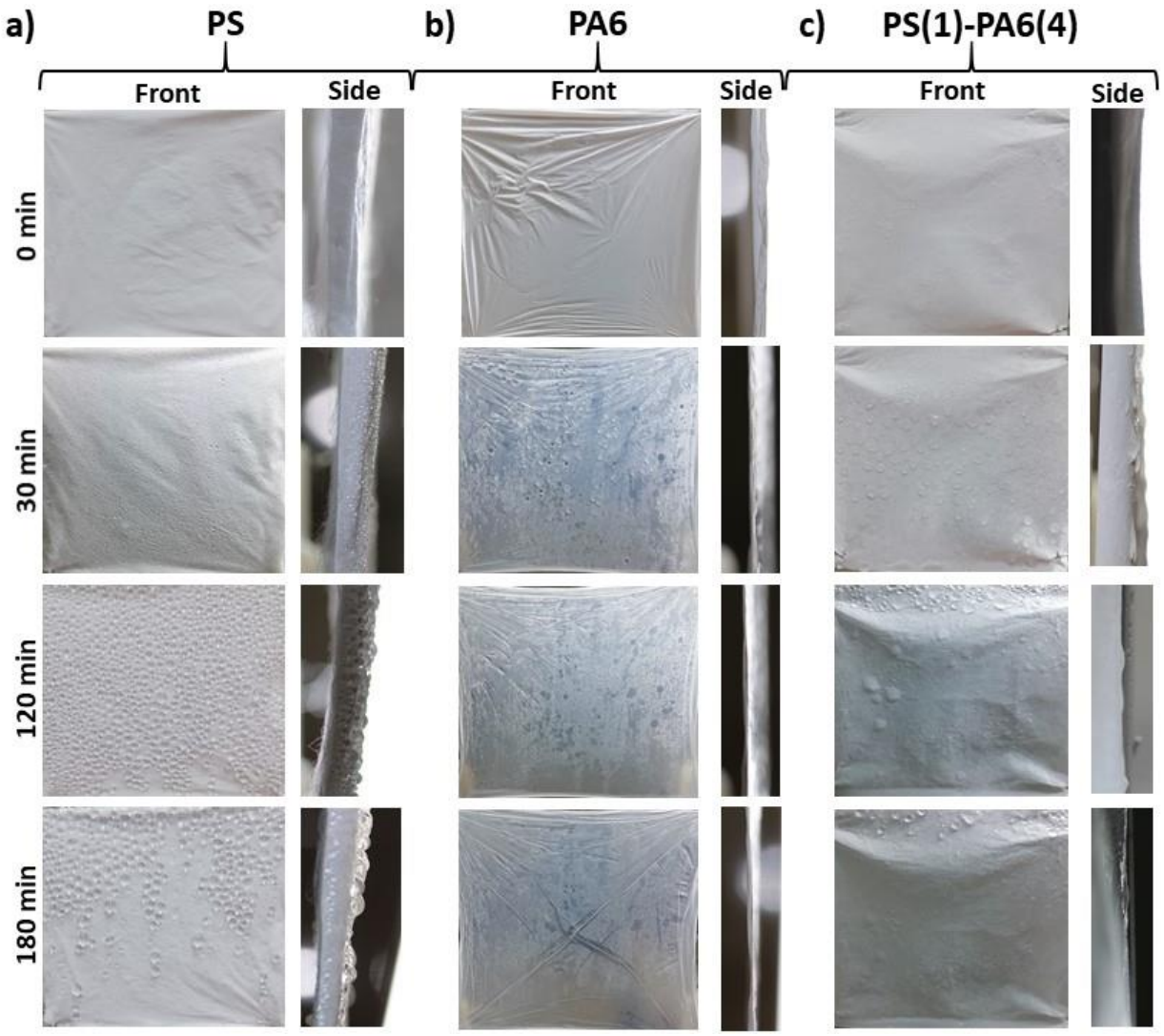

Figure 7. The front and side images of fibers meshes with collected water droplets for selected time of 0, 30, 120 and 180 minutes for a) PS mat, b) PA6 mat, c) PS(1)-PA6(4) composites.

During the experiments the water was weighed every 30 min to calculate the efficiency of composite meshes in collecting water, see Figure 8 b-d. The efficiency for composites has a linear profile in opposition to just PS mesh. The highest amount of water collected was for the PS(1)-PA6(4) composite. The obtained efficiency is often difficult to compare to previous studies as the experimental designs were different including also the collecting materials and surfaces[13,14,15,32]. In the first set of our experiments the distance between the mesh and the orifice from the humidifier was set to 15 cm in our experiments and the angle of the vapor stream falling on the meshes in the frame was 30º, see Figure 2b). This gives sufficient time for

the steam to condense on the fibers[14]. In reference to other studies, this distance was 5 cm[13] and 6 cm[32]. The larger distance enabled to water condensation on the entire surface of the mesh. The experiments were repeated for the PS(1)-PA6(4) composite with the shorter distance to prove the best performance of it, see Fig 2b) with the distance of 6 cm. The efficiency in collecting water from humid air was calculated as the mass of the collected water from the beaker placed under the mesh per unit area. Additionally, the mass of water captured between fibers in the mesh was also weighted. The total amount of water is graphically shown in Figure 8c per 1h and per total time of the experiment, 3h, in Figure 8d. The highest efficiency of water collected to the beaker is for the composite PS(1)-PA6(4) reaching 37.81 $mg \cdot cm^{-2} \cdot h^{-1}$ but a small amount of water was still in the nets (4.70 $mg \cdot cm^{-2} \cdot h^{-1}$). In previous studies it was only verified for up to 60 min where the efficiency was calculated for 3 mats: unimpregnated PVDF-HFP and impregnated by total quartz oil and Krytox-1506 [32], giving 77 to 118 $mg \cdot cm^{-2} h^{-1}$. The obtained values were slightly higher but the distance of the orifice from the humidify to the mesh was exactly close. Importantly the mesh required postprocessing after electrospinning to achieve increased efficiency in collecting water. For the case of only PS fibers, a lot of water stayed on the mesh due to its high hydrophobicity. Also, the process of collecting water is less effective for typical fog collector constructions. Water is typically collected in a spout and transferred to the tank[10]. The efficiency of commercial Fog Water Collectors is 3 – 10 $l \cdot m^{-2}$ from the mesh (with area of $40 m^2$) per day[22] and is highly deepened on the wind speed and weather conditions.

Our system based on hydrophobic and hydrophilic fibers allows to catch the fog and transport collected water droplets to the special container without additional surface modifications, using oil or lubricant, what reduces the danger of water contamination. The water collection experiments in our laboratory at humidity 95-99% for 6 cm distance and 90-95% for 15 cm distance, see Figure 2. In reference to *Lalia et al*[32] they conducted an experiment in the chamber with humidity of 70% and temperature of 20ºC using also a shorter

distance of only 6 cm, but *Azad et al*[14] kept it of 17 cm. Our results presented in Figure 9, show that the distance of humidifier to the meshes affect the water collection efficiency. We need to point out that in our experiment the fog flow velocity is lower in comparison to other studies. The higher fog flow velocity the more vapor will pass through the meshes in the given time and the more droplets will settle on the fibers. Our fibers mesh reached lower efficiency that to materials used by *Lalia et al*[32], but used by us fog flow velocity (19 $cm \cdot s^{-1}$) was almost half to use by their (40 $cm \cdot s^{-1}$). In comparison *Azad et al*[14] also used a higher fog flow velocity (160 $cm \cdot s^{-1}$). To indicate the huge effect of experimental conditions and water collection we performed addition experiments for the best performing mesh PS(1)-PA6(4) by reducing the distance to 6 cm using a 90º steam flow, see Figure 2b. As a consequence, the efficiency of collected water increased by more than 40% from 37.81 $mg \cdot cm^{-2} \cdot h^{-1}$ to 52.96 $mg \cdot cm^{-2} \cdot h^{-1}$, see Figure 9.

In the first set of experiments the fog flow was deliberately tilted to 30º because this setting largely limited the air movement imitating environmental conditions with low winds. For FWC applications it is the wind that actually results in the drainage of the water collected in the meshes. Our experimental system imitated the worst climate scenarios showing a wide range of applicability of the design by us with our PS – PA6 meshes, see Figure 9. In the repeated experiment for the PS(1)-PA6(4) composite the fog flow was set to an angle of 90º, which is closer to the real state in nature. The reduction in distance between the steam outlet and the nets caused an increase in efficiency in water collection. For the same experimental settings, we compared efficiency of collecting water for the composite with the best wetting and mechanical properties with a commercial Raschel mesh used in FWC constructions (Figure 9). Independence from the distance between the fog flow and the mesh, the PS(1)-PA6(4) composite shows much higher efficiency to collect water than the Raschel mesh by more than 131% (15 cm) and 224% (6 cm). This indicates the potential application for use of these fibers' composites in existing constructions.

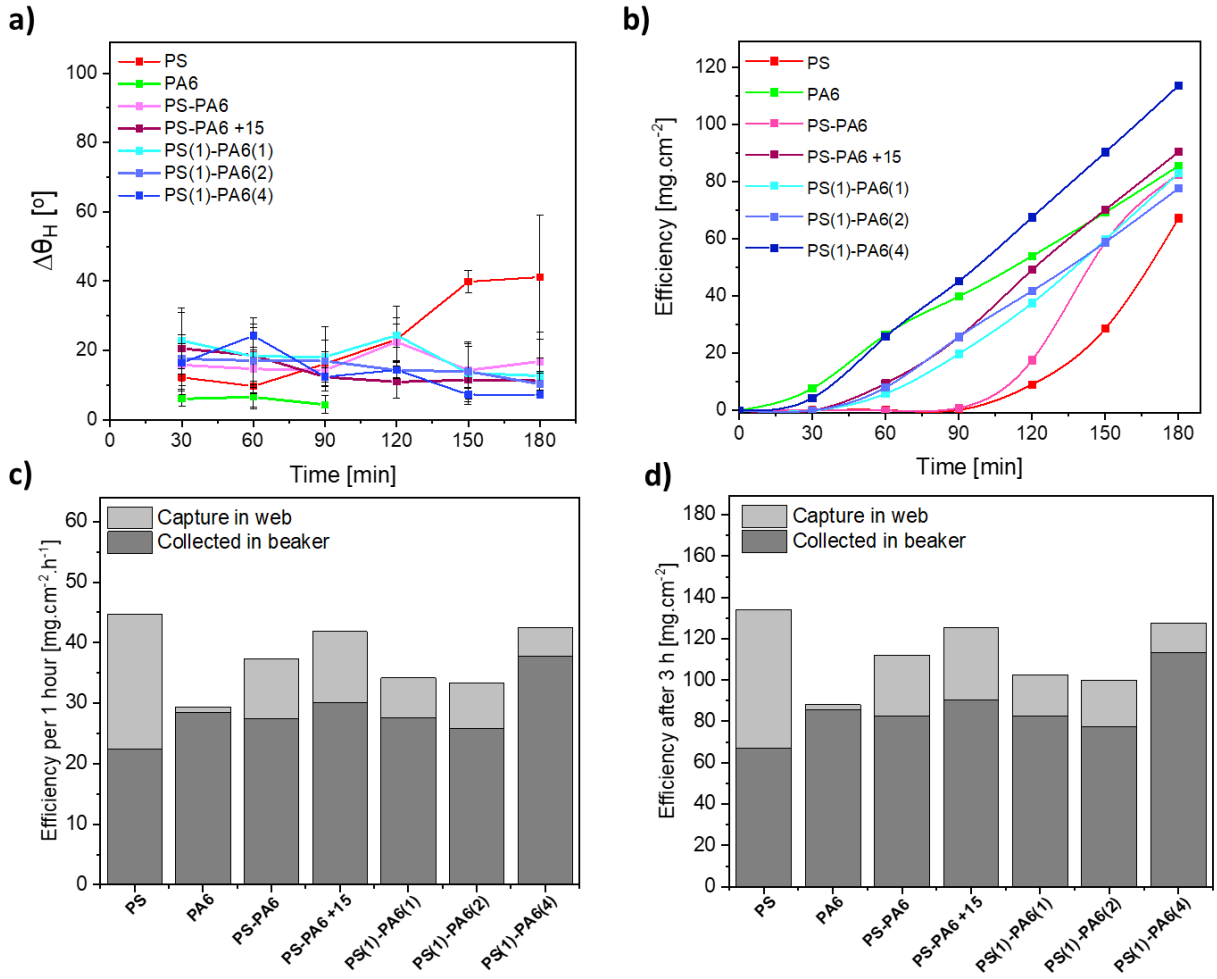

Figure 8. The changes of angles of hysteresis (a) and efficiency of collected water (b, c, d) on electrospun samples, for the distance of 15 cm between humidifier and mesh and angle of 30º.

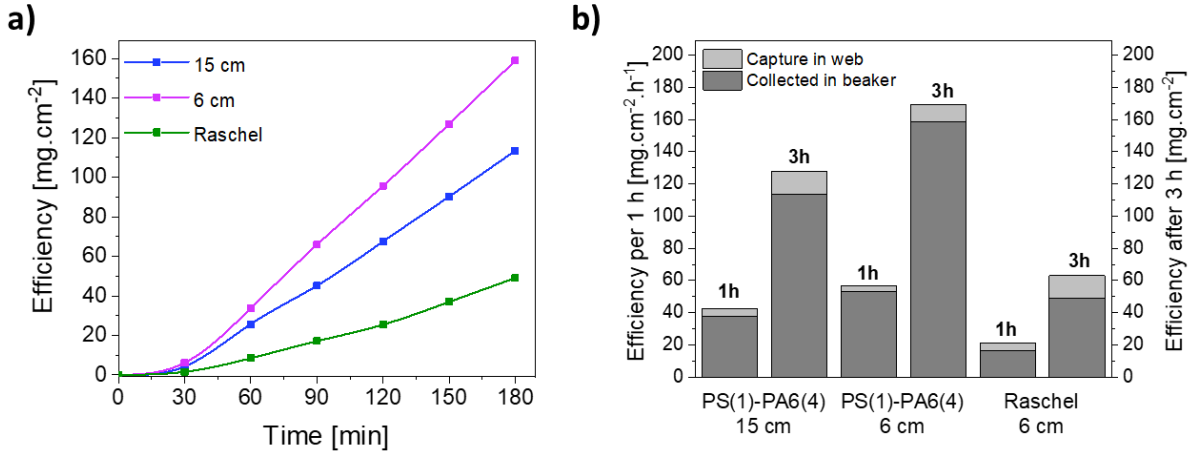

Figure 9. The efficiency of collecting water for composite PS(1)-PA6(4) according to experimental condition such as humidifier distance to mesh of 6 and 15 cm and angle of 90º in commission to Raschel mesh tested with humidifier at 6 cm.

The combination of hydrophobic and hydrophilic fibers appears to play a crucial role in increasing the efficiency in collecting water[44]. The condensation of water droplets is more effectively obtained for hydrophilic surfaces as indicated in nature[45], where the hydrophobic fraction allowing droplets to roll over for the collection[46]. Purely hydrophobic meshes keep the droplets on their surfaces for too long, blocking the meshes even with continuous wind being blown thus preventing the collection of new water droplets, therefore their efficiency is reduced[10]. For the cases of composite meshes, containing the highest hydrophilic fractions, droplets are trapped between fibers, thus impeding their collection[47]. Therefore, the key to design of effective meshes for water collection is a combination of hydrophobic and hydrophilic materials[7,44]. This is what is illustrated by the scheme in Figure 10. We can observe 3 main steps during water collection experiments which are: 1 – the droplets deposition on fibers; 2 – droplets start to accumulate; and 3 – collected droplets integrate and form larger droplets, reducing the number of smaller droplets. The mechanism of larger and heavier droplets allows a faster and easier sliding process of the water on the surface. This is particularly true for meshes containing hydrophilic nanofibers such as a composite of PS(1)-PA6(4) possessing decreased roughness and hydrophobicity. The right balance of hydrophobic and hydrophilic interaction between solid surface matters together with controlled geometry. These two parameters are the key to obtaining an efficient mechanism of collecting water from meshes as indicated in Figure 10. Additionally, in Figure 11, the schematics of the side view of the collected water droplets attachment and sliding steps on the meshes are presented. The hydrophilic fraction of PA6 nanofibers accelerates the droplets sliding by reducing the contact angle hysteresis, as it is shown in the experimental data presented in Figure 8a. It is in opposition to hydrophobic PS fibers, where the droplets are disattached from the mesh after reaching the critical volume or mass allowing the gravitational force to push it down to the beaker. In nature winds simply shakes it off. The mechanism of the enhancement of fog collection for composite illustrated in Figure 10 and 11 shows also the importance of PS

microfibers fraction which prevent the water droplets from penetrating the composite mesh. The hydrophilic meshes build of only PA6 nanofibers are trapping the water droplets between fibers as demonstrated in Figure S4a in the Supporting Information, what reduces the efficiency in collecting water, see also schematics and image in Figure 10 b.

Based on our previous research[31] we undertook a comprehensive study about the influence of the fibers' diameter in relation to static water contact angle to PMMA electrospun fibers with 3 different average diameters (0.30 µm, 1.43 µm, 2.57 µm). The changes of these diameters did not show any significant differences between water contact angle. In conclusion the water contact angle hysteresis strongly depends on the hydrophobic and the hydrophilic properties of the fibers.

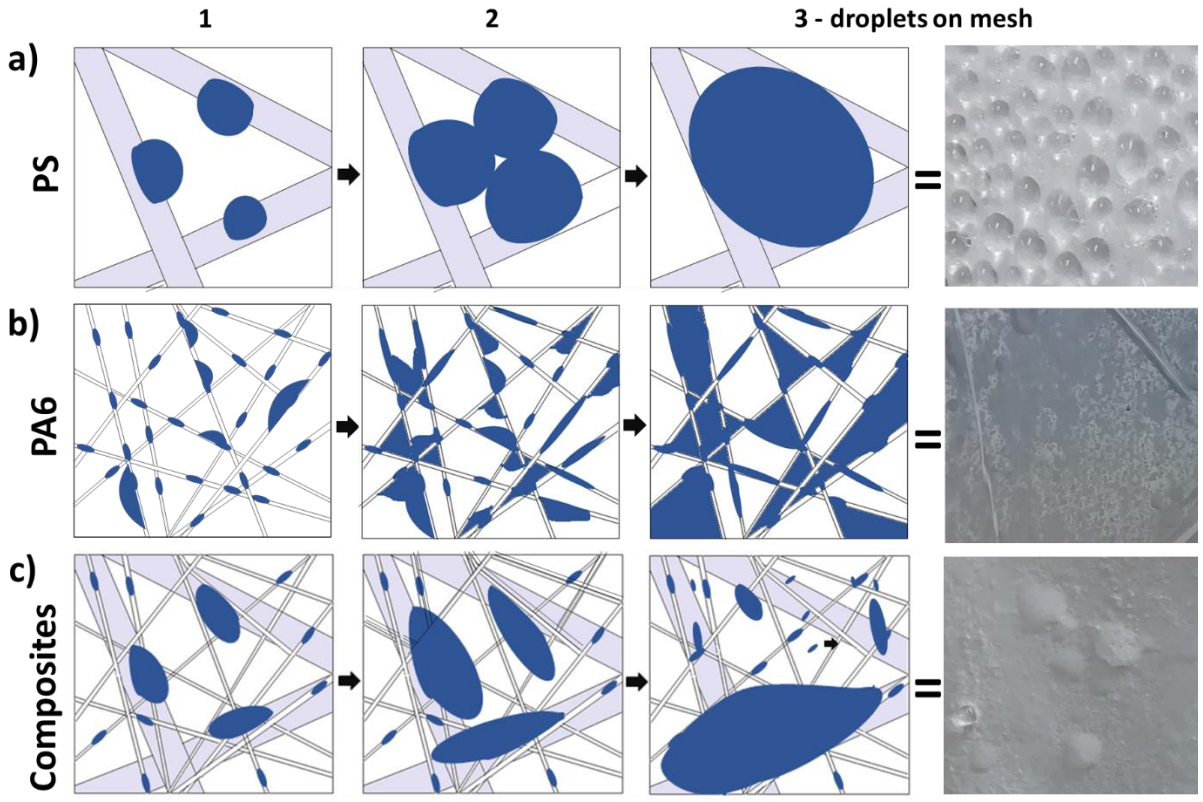

Figure 10. Illustrations of collecting water droplets on different electrospun meshes: a) growing droplets on hydrophobic PS microfibers, b) droplets inputting between hydrophilic PA6 nanofibers, c) droplets growing and running down a composite mesh.

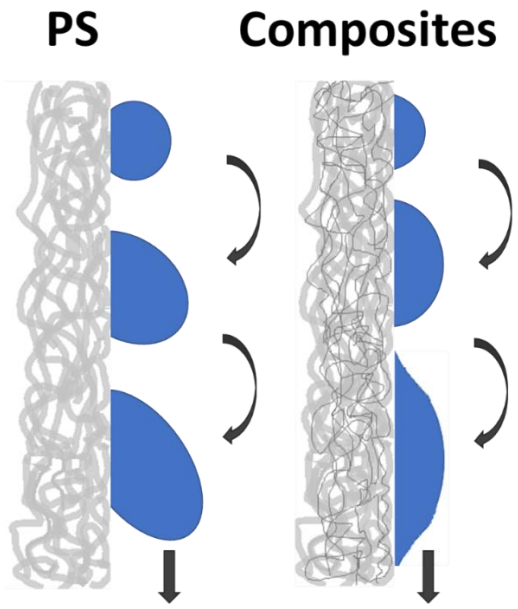

Figure 11. Schematics of droplet of water collection and dispatchment on illustrating the mechanism of droplets moving down on the hydrophobic PS and hydrophobic PS – hydrophilic PA6 composites meshes.

4. CONCLUSION

Composites consisting of hydrophobic and hydrophilic fibers were successfully fabricated using a two-nozzle electrospinning set-up. A range of parameters were considered in order to design an optimal mesh for the harvesting of water from fog. We have demonstrated and explained, that it is possible to control the fraction of hydrophobic and hydrophilic fraction in composites. This, in turn is able to modify the wetting, roughness and strength properties in a single step of the manufacturing process. The best performance was achieved for the composite PS(1)-PA6(4) in terms of the efficiency in collecting water over 3 hours. This reached 127.55 $mg \cdot cm^{-2}$ and with mechanical properties (σ_{max}= 0.11 ± 0.01 MPa), which are important to survive windy environments. It is the first time we present this detailed study showing the water collection changes over a few hours and explain the mechanism that enhances the efficiency in water collection on electrospun fiber composites. We have exploited a new concept of producing fibrous composite meshes to achieve a droplet sliding mechanism to

collect water by accelerating the droplet coalescence. The combination of hydrophobic and hydrophilic fraction and macro- and nano- sized fibers with controlling roughness enables the most effective mechanism in water collection. The higher fraction of PA6 reduces the roughness of meshes allowing the directional transport of water for application to FWC in order to increase their efficiency in collecting water. We have shown the applicability of the approach to changing existing FWCs by incorporating electrospun composite meshes with controlled mechanical and wetting properties. Future studies include the modification of a commercially available FWC and laboratory tests of their efficiency in water collection. Electrospun fibers show a great application potential with existing FWC in water harvesting to increase their efficiency.

ACKNOWLEDGMENTS

We would like to thank to Prof. Otto Klemm from University of Münster in Germany for sharing with us the commercial Raschel mesh used in FWC constructions. The study was conducted with the funding from the SONATA BIS 5 project grant provided by the National Science Centre in Poland. No 2015/18/E/ST5/00230.

Supporting Information include the following information:

Experimental setup for tensile testing of electrospun fibers; profilometry study of electrospun meshes; advancing contact angle measurements; contact angle data with rain water; micrographs from Environmental Scanning Electron Microscope (ESEM); SEM images of fibrous meshes after collecting water droplets from humid air; images of water droplets on commercial Raschel mesh.

REFERENCES

(1) Andersen, H.; Cermak, J. First Fully Diurnal Fog and Low Cloud Satellite Detection

Reveals Life Cycle in the Namib. *Atmospheric Measurement Techniques* **2018**, *11* (10), 5461–5470. https://doi.org/10.5194/amt-11-5461-2018.

(2) Lehnert, L. W.; Thies, B.; Trachte, K.; Achilles, S.; Osses, P.; Baumann, K.; Schmidt, J.; Samolov, E.; Jung, P.; Leinweber, P.; Karsten, U.; Büdel, B.; Bendix, J. A Case Study on Fog/Low Stratus Occurrence at Las Lomitas, Atacama Desert (Chile) as a Water Source for Biological Soil Crusts. *Aerosol and Air Quality Research* **2018**, *18* (1), 254–269. https://doi.org/10.4209/aaqr.2017.01.0021.

(3) Wang, W.; Xu, W.; Collett, J. L.; Liu, D.; Zheng, A.; Dore, A. J.; Liu, X. Chemical Compositions of Fog and Precipitation at Sejila Mountain in the Southeast Tibetan Plateau, China. *Environmental Pollution* **2019**, *253*, 560–568. https://doi.org/10.1016/j.envpol.2019.07.055.

(4) Baji, A.; Abtahi, M.; Ramakrishna, S. Bio-Inspired Electrospun Micro/Nanofibers with Special Wettability. *Journal of Nanoscience and Nanotechnology* **2014**, *14* (7), 4781–4798. https://doi.org/10.1166/jnn.2014.8841.

(5) Hou, Y.; Chen, Y.; Xue, Y.; Zheng, Y.; Jiang, L. Water Collection Behavior and Hanging Ability of Bioinspired Fiber. *Langmuir* **2012**, *28* (10), 4737–4743. https://doi.org/10.1021/la204682j.

(6) Zheng, Y.; Bai, H.; Huang, Z.; Tian, X.; Nie, F. Q.; Zhao, Y.; Zhai, J.; Jiang, L. Directional Water Collection on Wetted Spider Silk. *Nature* **2010**, *463* (7281), 640–643. https://doi.org/10.1038/nature08729.

(7) Brown, P. S.; Bhushan, B. Bioinspired Materials for Water Supply and Management: Water Collection, Water Purification and Separation of Water from Oil. *Philosophical Transactions of the Royal Society A: Mathematical, Physical and Engineering Sciences* **2016**, *374* (2073). https://doi.org/10.1098/rsta.2016.0135.

(8) Mayerhofer, M.; Loster, T. IntoAction Nebelnetze. **2015**, No. November.

(9) Rivera, J. D. D.; Lopez-Garcia, D. Mechanical Characteristics of Raschel Mesh and Their Application to the Design of Large Fog Collectors. *Atmospheric Research* **2015**, *151*, 250–258. https://doi.org/10.1016/j.atmosres.2014.06.011.

(10) Fernandez, D. M.; Torregrosa, A.; Weiss-Penzias, P. S.; Zhang, B. J.; Sorensen, D.; Cohen, R. E.; McKinley, G. H.; Kleingartner, J.; Oliphant, A.; Bowman, M. Fog Water Collection Effectiveness: Mesh Intercomparisons. *Aerosol and Air Quality Research* **2017**, *18* (1), 270–283. https://doi.org/10.4209/aaqr.2017.01.0040.

(11) Xue, J.; Wu, T.; Dai, Y.; Xia, Y. Electrospinning and Electrospun Nanofibers: Methods, Materials, and Applications. *Chemical Reviews* **2019**, *119* (8), 5298–5415. https://doi.org/10.1021/acs.chemrev.8b00593.

(12) Dong, H.; Wang, N.; Wang, L.; Bai, H.; Wu, J.; Zheng, Y.; Zhao, Y.; Jiang, L. Bioinspired Electrospun Knotted Microfibers for Fog Harvesting. *ChemPhysChem* **2012**, *13* (5), 1153–1156. https://doi.org/10.1002/cphc.201100957.

(13) Ganesh, V. A.; Ranganath, A. S.; Baji, A.; Raut, H. K.; Sahay, R.; Ramakrishna, S. Hierarchical Structured Electrospun Nanofibers for Improved Fog Harvesting Applications. *Macromolecular Materials and Engineering* **2017**, *302* (2), 1–7. https://doi.org/10.1002/mame.201600387.

(14) Azad, M. A. K.; Krause, T.; Danter, L.; Baars, A.; Koch, K.; Barthlott, W. Fog Collection on Polyethylene Terephthalate (PET) Fibers: Influence of Cross Section and Surface Structure. *Langmuir* **2017**, *33* (22), 5555–5564. https://doi.org/10.1021/acs.langmuir.7b00478.

(15) Zhong, L.; Zhang, R.; Li, J.; Guo, Z.; Zeng, H. Efficient Fog Harvesting Based on 1D Copper Wire Inspired by the Plant Pitaya. *Langmuir* **2018**, *34* (50), 15259–15267.

https://doi.org/10.1021/acs.langmuir.8b03418.

(16) Shi, W.; Anderson, M. J.; Tulkoff, J. B.; Kennedy, B. S.; Boreyko, J. B. Fog Harvesting with Harps. *ACS Applied Materials & Interfaces* **2018**, *10* (14), 11979–11986. https://doi.org/10.1021/acsami.7b17488.

(17) Li, C.; Liu, Y.; Gao, C.; Li, X.; Xing, Y.; Zheng, Y. Fog Harvesting of a Bioinspired Nanocone-Decorated 3D Fiber Network. *ACS Applied Materials and Interfaces* **2019**, *11* (4), 4507–4513. https://doi.org/10.1021/acsami.8b15901.

(18) Gurera, D.; Bhushan, B. Optimization of Bioinspired Conical Surfaces for Water Collection from Fog. *Journal of Colloid and Interface Science* **2019**, *551*, 26–38. https://doi.org/10.1016/j.jcis.2019.05.015.

(19) Ang, B. T. W.; Zhang, J.; Lin, G. J.; Wang, H.; Lee, W. S. V.; Xue, J. Enhancing Water Harvesting through the Cascading Effect. *ACS Applied Materials & Interfaces* **2019**, acsami.9b08460. https://doi.org/10.1021/acsami.9b08460.

(20) Orejon, D.; Askounis, A.; Takata, Y.; Attinger, D. Dropwise Condensation on Multiscale Bioinspired Metallic Surfaces with Nanofeatures. *ACS Applied Materials & Interfaces* **2019**, *11*, 24735–24750. https://doi.org/10.1021/acsami.9b06001.

(21) Damak, M.; Varanasi, K. K. Electrostatically Driven Fog Collection Using Space Charge Injection. *Science Advances* **2018**, *4* (6), 1–9. https://doi.org/10.1126/sciadv.aao5323.

(22) Klemm, O.; Schemenauer, R. S.; Lummerich, A.; Cereceda, P.; Marzol, V.; Corell, D.; Van Heerden, J.; Reinhard, D.; Gherezghiher, T.; Olivier, J.; Osses, P.; Sarsour, J.; Frost, E.; Estrela, M. J.; Valiente, J. A.; Fessehaye, G. M. Fog as a Fresh-Water Resource: Overview and Perspectives. *Ambio* **2012**, *41* (3), 221–234. https://doi.org/10.1007/s13280-012-0247-8.

(23) Schemenauer, R. S.; Cereceda, P. The Role of Wind in Rainwater Catchment and Fog Collection. *Water International* **1994**, *19* (2), 70–76. https://doi.org/10.1080/02508069408686203.

(24) Kurusu, R. S.; Demarquette, N. R. Surface Modification to Control the Water Wettability of Electrospun Mats. *International Materials Reviews* **2019**, *64* (5), 249–287. https://doi.org/10.1080/09506608.2018.1484577.

(25) Duprat, C.; Protière, S.; Beebe, A. Y.; Stone, H. A. Wetting of Flexible Fibre Arrays. *Nature* **2012**, *482* (7386), 510–513. https://doi.org/10.1038/nature10779.

(26) Yoon, J. W.; Park, Y.; Kim, J.; Park, C. H. Multi-Jet Electrospinning of Polystyrene/Polyamide 6 Blend: Thermal and Mechanical Properties. *Fashion and Textiles*. 2017. https://doi.org/10.1186/s40691-017-0090-4.

(27) Cui, H.; Li, Y.; Zhao, X.; Yin, X.; Yu, J.; Ding, B. Multilevel Porous Structured Polyvinylidene Fl Uoride / Polyurethane Fi Brous Membranes for Ultrahigh Waterproof and Breathable Application. *Composites Communications* **2017**, *6* (October), 63–67. https://doi.org/10.1016/j.coco.2017.10.002.

(28) Chiverton, J. P.; Tozzi, G. Automatic Diameter and Orientation Distribution Determination of Fibrous Materials in Micro X-Ray CT Imaging Data. *Journal of microscopy* **2018**, 1–16. https://doi.org/10.1111/jmi.12719.

(29) Frangi, A. F.; Niessen, W. J.; Vincken, K. L.; Viergever, M. A. Multiscale Vessel Enhancement Filtering *. *International Conference on Medical Image Computing and Computer-Assisted Intervention* **1998**, 130–137.

(30) Antiga, L. Generalizing Vesselness with Respect to Dimensionality and Shape. *The Insight Journal* **2007**, 3, 1–14.

(31) Szewczyk, P. K.; Ura, D. P.; Metwally, S.; Knapczyk-Korczak, J.; Gajek, M.; Marzec, M. M.; Bernasik, A.; Stachewicz, U. Roughness and Fiber Fraction Dominated Wetting of Electrospun Fiber-Based Porous Meshes. *Polymers* **2019**, *11* (1), 34. https://doi.org/10.3390/polym11010034.

(32) Lalia, B. S.; Anand, S.; Varanasi, K. K.; Hashaikeh, R. Fog-Harvesting Potential of Lubricant-Impregnated Electrospun Nanomats. *Langmuir* **2013**, *29* (42), 13081–13088. https://doi.org/10.1021/la403021q.

(33) Schemenauer, R. S.; Cereceda, P. Fog-Water Collection in Arid Coastal Locations. *Ambio* **1991**, *20* (7), 303–308.

(34) Schemenauer, R. S.; Cereceda, P. A Proposed Standard Fog Collector for Use in High-Elevation Regions. *Journal of Applied Meteorology* **1994**, *33* (11), 1313–1322. https://doi.org/10.1175/1520-0450(1994)033<1313:APSFCF>2.0.CO;2.

(35) Pai, C. L.; Boyce, M. C.; Rutledge, G. C. Morphology of Porous and Wrinkled Fibers of Polystyrene Electrospun from Dimethylformamide. *Macromolecules* **2009**, *42* (6), 2102–2114. https://doi.org/10.1021/ma802529h.

(36) Bonino, C. A.; Efimenko, K.; Jeong, S. I.; Krebs, M. D.; Alsberg, E.; Khan, S. A. Three-Dimensional Electrospun Alginate Nanofiber Mats via Tailored Charge Repulsions. *Small* **2012**, *8* (12), 1928–1936. https://doi.org/10.1002/smll.201101791.

(37) Stachewicz, U.; Bailey, R. J.; Zhang, H.; Stone, C. A.; Willis, C. R.; Barber, A. H. Wetting Hierarchy in Oleophobic 3D Electrospun Nanofiber Networks. *ACS Applied Materials and Interfaces* **2015**, *7* (30), 16645–16652. https://doi.org/10.1021/acsami.5b04272.

(38) Stachewicz, U.; Barber, A. H. Enhanced Wetting Behavior at Electrospun Polyamide Nanofiber Surfaces. *Langmuir* **2011**, *27* (6), 3024–3029.

https://doi.org/10.1021/la1046645.

(39) Zhang, F.; Barber, A. H. Extreme Toughness Exhibited in Electrospun Polystyrene Fibers. *Macromolecular Materials and Engineering* **2017**, *302* (9), 1–7. https://doi.org/10.1002/mame.201700084.

(40) Li, X.; Ding, B.; Lin, J.; Yu, J.; Sun, G. Enhanced Mechanical Properties of Superhydrophobic Microfibrous Polystyrene Mats via Polyamide 6 Nanofibers. *The Journal of Physical Chemistry C* **2009**, *113* (47), 20452–20457. https://doi.org/10.1021/jp9076933.

(41) Bhushan, B.; Chae Jung, Y. Wetting Study of Patterned Surfaces for Superhydrophobicity. *Ultramicroscopy* **2007**, *107* (10–11), 1033–1041. https://doi.org/10.1016/j.ultramic.2007.05.002.

(42) Ma, M.; Hill, R. M.; Rutledge, G. C. A Review of Recent Results on Superhydrophobic Materials Based on Micro- and Nanofibers. *Journal of Adhesion Science and Technology* **2008**, *22* (15), 1799–1817. https://doi.org/10.1163/156856108X319980.

(43) Ma, M.; Gupta, M.; Li, Z.; Zhai, L.; Gleason, K. K.; Cohen, R. E.; Rubner, M. F.; Rutledge, G. C. Decorated Electrospun Fibers Exhibiting Superhydrophobicity. *Advanced Materials* **2007**, *19* (2), 255–259. https://doi.org/10.1002/adma.200601449.

(44) Chen, D.; Li, J.; Zhao, J.; Guo, J.; Zhang, S.; Sherazi, T. A.; Ambreen; Li, S. Bioinspired Superhydrophilic-Hydrophobic Integrated Surface with Conical Pattern-Shape for Self-Driven Fog Collection. *Journal of Colloid and Interface Science* **2018**, *530*, 274–281. https://doi.org/10.1016/j.jcis.2018.06.081.

(45) Bhushan, B. Biomimetics: Lessons from Nature - an Overview. *Philosophical Transactions of the Royal Society A: Mathematical, Physical and Engineering Sciences* **2009**, *367* (1893), 1445–1486. https://doi.org/10.1098/rsta.2009.0011.

(46) Bhushan, B.; Jung, Y. C.; Koch, K. Micro-, Nano- And Hierarchical Structures for Superhydrophobicity, Self-Cleaning and Low Adhesion. *Philosophical Transactions of the Royal Society A: Mathematical, Physical and Engineering Sciences* **2009**, *367* (1894), 1631–1672. https://doi.org/10.1098/rsta.2009.0014.

(47) Cao, M.; Xiao, J.; Yu, C.; Li, K.; Jiang, L. Hydrophobic/Hydrophilic Cooperative Janus System for Enhancement of Fog Collection. *Small* **2015**. https://doi.org/10.1002/smll.201500647.

TOC Graphic

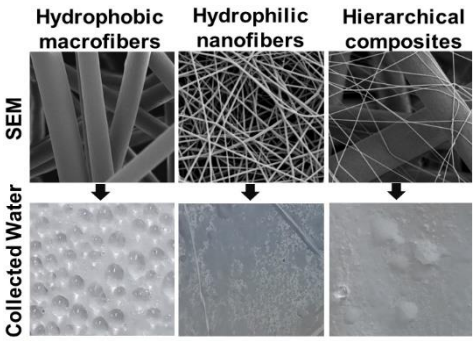
Hydrophobic macrofibers
Hydrophilic nanofibers
Hierarchical composites
SEM
Collected Water